High-resolution imaging of compact high-velocity clouds

Heij, V. de; Braun, R.; Burton, W.B.

A&A 391, 67–81 (2002)
DOI: 10.1051/0004-6361:20020640

Astronomy & Astrophysics

High–resolution imaging of compact high–velocity clouds

V. de Heij[1], R. Braun[2], and W. B. Burton[1,3]

[1] Sterrewacht Leiden, PO Box 9513, 2300 RA Leiden, The Netherlands
[2] Netherlands Foundation for Research in Astronomy, PO Box 2, 7990 AA Dwingeloo, The Netherlands
[3] National Radio Astronomy Observatory, 520 Edgemont Road, Charlottesville, Virginia 22903, USA

Received 14 March 2002 / Accepted 24 April 2002

Abstract. We have imaged five compact high–velocity clouds in H I with arcmin angular resolution and km s^{-1} spectral resolution using the Westerbork Synthesis Radio Telescope. These CHVCs have a characteristic morphology, consisting of one or more quiescent, low–dispersion compact cores embedded in a diffuse warm halo. The compact cores can be unambiguously identified with the cool neutral medium of condensed atomic hydrogen, since their linewidths are significantly narrower than the thermal linewidth of the warm neutral medium. Because of the limited sensitivity to diffuse emission inherent to interferometric data, the warm medium is not directly detected in the WSRT observations. Supplementary total–power data, which is fully sensitive to both the cool and warm components of H I, is available for comparison for all the sources, albeit with angular resolutions that vary from 3′ to 36′. The fractional H I flux in compact CNM components varies from 4% to 16% in our sample. All objects have at least one local peak in the CNM column density which exceeds about 10^{19} cm^{-2} when observed with arcmin resolution. It is plausible that a peak column density of $1–2 \times 10^{19}$ cm^{-2} is a prerequisite for the long–term survival of these sources. One object in our sample, CHVC 120−20−443 (Davies' cloud), lies in close projected proximity to the disk of M 31. This object is characterized by exceptionally broad linewidths in its CNM concentrations, more than 5 times greater than the median value found in the 13 CHVCs studied to date at comparable resolution. These CNM concentrations lie in an arc on the edge of the source facing the M 31 disk. The diffuse H I component of this source, seen in total–power data from the NRAO 140–foot telescope, has a positional offset in the direction of the M 31 disk. All of these attributes suggest that CHVC 120−20−443 is in a different evolutionary state than most of the other CHVCs which have been studied. Similarly broad CNM linewidths have only been detected in one other cloud, CHVC 110.6−07.0−466 (Wakker & Schwarz 1991) which also lies in the Local Group barycenter direction and has the most extreme radial velocity known. A distinct possibility for Davies' cloud seems to be physical interaction of some type with M 31. The most likely form of this interaction might be the ram–pressure or tidal–stripping by either one of M 31's visible dwarf companions, M 32 or NGC 205, or else by a dark companion with an associated H I condensation. The compact objects located in the direction of the Local Group barycenter have an important role to play in constraining the Local Group hypothesis for the deployment of CHVCs.

Key words. ISM: atoms – ISM: clouds – Galaxy: evolution – Galaxy: formation – galaxies: dwarf – galaxies: Local Group

1. Introduction

Although high–velocity clouds have been studied extensively since their discovery in 1963 by Muller et al. (1963), there is still no consensus on the origin and physical properties of these objects. The clouds, for which most of the observations have been done in the H I 21–cm emission line, have velocities in excess of those allowed by Galactic rotation. Most of the physical properties like size, mass, and gas density depend sensitively on the distances of the clouds: these distances are still unknown, except in a few cases. The Magellanic Stream represents tidal debris originating in the gravitational interaction of the Large and Small Magellanic Clouds with our Galaxy (see Putman & Gibson 1999). The Stream is therefore likely located at a distance of about 50 kpc. Other high–velocity features with constrained distances are a few large complexes, extending over some tens of square degrees. One of these, Complex A, has been found from absorption–line observations (van Woerden et al. 1999; Wakker 2001) to lie within the distance range of $8 < d < 10$ kpc. Wakker & van Woerden (1997) and Wakker et al. (1999) have given recent reviews of the high–velocity cloud phenomenon.

During the past several years, there has been a renewed interest in the possibility that many high–velocity clouds are scattered throughout the Local Group. This hypothesis has been considered by many authors over the past decades: although some of the earlier references now appear somewat outdated, several early studies seem to have been particularly presentient: these include the work of Verschuur (1969), who discussed high–velocity clouds as protogalactic material scattered throughout the Local Group, and the work of Eichler (1976) and Einasto et al. (1976), who viewed high–velocity clouds

Send offprint requests to: R. Braun,
e-mail: rbraun@astron.nl

as carriers of dark matter, also scattered throughout the Local Group and available for merger with the larger systems.

Cosmological simulations intended to represent the evolution of the Local Group now predict a much higher number of dark–matter satellites around our Galaxy and Andromeda than the number of observed dwarf galaxies (Klypin et al. 1999; Moore et al. 1999). Although there are several possible solutions to this problem, one is that the missing dark matter satellites should not only be identified with dwarf galaxies, but also with the high–velocity clouds. These objects would have a very low star–formation rate, consistent with the non–detection of stars or of emission from dust or molecules associated with pre–stellar conditions. Whereas Blitz et al. (1999) considered the properties of a general high–velocity cloud catalog in search of evidence for this hypothesis, Braun & Burton (1999) restricted their study to the compact and isolated ones, the so-called CHVCs. These objects are isolated in the sense that they are not connected to extended emission features at a level of $N_{\rm HI} = 1.5 \times 10^{18}\,{\rm cm}^{-2}$. Such isolated objects turn out to be very compact, having a median angular size of less than 1°. The signature of these small and compact clouds in the Leiden/Dwingeloo survey (LDS, Hartmann & Burton 1997) is indistinguishable from that of a nearby dwarf galaxy. If the high–velocity clouds are the baryonic counterparts of low–mass dark–matter halos, then the subset of compact and isolated objects would be the most likely candidates for clouds at substantial distances, as yet undistorted by tidal– and ram–pressure stripping.

The visual search for CHVCs of Braun & Burton (1999) in the LDS data has been extended by de Heij et al. (2002a), with a fully automated algorithm. The same algorithm was used to isolate the CHVC population in the southern hemisphere from the HIPASS data by Putman et al. (2002). The velocity dispersion of these compact and isolated clouds is the lowest in the Local Group Standard of rest system, lending some support to the idea that they are located throughout the Local Group. More importantly, self–consistent modeling of H I bound to a dark–matter mini–halo population in the Local Group potential carried out by de Heij et al. (2002b) gives support to this scenario. Critical aspects of this modeling are the realistic treatment of the effects of foreground obscuration by the H I of our Galaxy, and the account taken of the limited resolution and sensitivity of the existing survey data.

Due to its limited spatial resolution of $36'$ *FWHM*, the Leiden/Dwingeloo survey is not an ideal basis for the study of the internal H I properties of the compact, high–velocity clouds. Braun & Burton (2000) obtained high–resolution WSRT observations of six of these clouds. Other than the work by Braun & Burton and that reported here, only two CHVCs had previously been imaged at high resolution, by Wakker & Schwarz (1991). The synthesis observations reveal a characteristic morphology in which one or more compact cores are embedded in a diffuse halo, confirming the results from single–dish work done on large telescopes at moderately high angular resolution, notably in the earlier work done on the NRAO 300–foot telescope, whose *FWHM* beam subtended 10 arcmin at λ21 cm, by Giovanelli et al. (1973). The narrow line widths characteristic of most core components seen at arcminute resolution in the synthesis data allow unambiguous identification of these with the cool condensed phase of HI, the CNM, with kinematic temperatures near 100 K. One of the CHVCs observed by Braun & Burton (2000), CHVC 125+41−207, showed several opaque clumps with some of the narrowest H I emission lines ever observed, with intrinsic *FWHM* of no more than 2 km s^{-1} and brightness temperature of 75 K. From a comparison of column and volume density for this object, Braun & Burton estimate a distance in the range 0.5 to 1 Mpc. In addition, several of the compact cores show systematic velocity gradients along the major axis of their elliptical extent. Some of these are well–fit by circular rotation in a flattened disk system. The apparent rotation velocities imply dark–matter masses of about $10^8\,M_\odot$ and dark–to–visible mass ratios of 10–50 or more. The cores of the multi–core objects show relative velocities as large as 70 km s^{-1} on 30 arcmin scales, also implying either an extremely short dynamically lifetime or a high dark–to–visible mass ratio.

In this paper, we extend the high–resolution study of CHVCs by imaging an additional five clouds with the WSRT. Our discussion is organized as follows. We begin by describing the method of sample selection in Sect. 2, proceed with a description of the newly acquired observations in Sect. 3, continue with a presentation of the images in Sect. 4, and conclude with discussion of our results in Sect. 5.

2. Sample selection

The sample was drawn from the CHVC catalog of de Heij et al. (2002a), which extends the original CHVC catalog produced by Braun & Burton (1999). Both catalogs are based on candidates extracted from the Leiden/Dwingeloo survey, after obtaining independent confirming data for each object. Braun & Burton (2000) selected a sample of six CHVCs for high–resolution WSRT imaging that spanned as wide a range in object parameters as possible. In particular, the selected sources varied in H I linewidth from as little as 6 km s^{-1} to as much as 95 km s^{-1} *FWHM*, while the median CHVC linewidth is about 30 km s^{-1}. The current sample of five additional objects was chosen to supplement this earlier one by targeting CHVCs with a relatively narrow velocity width and a moderately high peak brightness. This selection was motivated by the hope of detecting more examples of the extremely compact, high–column–density clumps found by Braun & Burton in CHVC 125+41−207. Resolved detection of such clumps allows meaningful distance constraints to be placed on the object.

Table 1 lists the basic properties of the CHVCs selected for WSRT imaging and discussed here. The velocity *FWHM* refers to the LDS spectrum with the peak brightness. The tabulated integrated fluxes also were determined from the LDS data (de Heij et al. 2002a), except in the case of CHVC 120−20−443, which extends in velocity beyond the LDS coverage. In this case, the Green Bank 140–foot observations described below were used. CHVC 120−20−443 is especially interesting in that it is located only 2° from the nuclear position of M 31, and has an extreme radial velocity exhibited by only a few CHVCs, all of which lie in the same general region, near the direction of the barycenter of the Local

Table 1. Basic properties of the sample of CHVCs imaged with the WSRT, based on data from the Leiden/Dwingeloo survey and additional observations. The velocity *FWHM* pertains to the LDS spectrum with the indicated peak brightness. The flux density of CHVC 120−20−443 refers to observations made with the Green Bank 140–foot telescope.

Object	RA (2000)	Dec (2000)	LDS structure	T_{max}	*FWHM*	total flux
CHVC *lll* ± *bb* ± *vvv*	(h m)	(° ′)	(a × b @ PA)	(K)	(km s^{-1})	(Jy km s^{-1})
CHVC 120−20−443	00 38.2	+42 28	0.°4 × 0.°4	0.29	18	95
CHVC 129+15−295	02 33.2	+76 40	0.°8 × 0.°8	0.44	18	120
CHVC 148−82−258	01 05.0	−20 16	0.°8 × 0.°8	0.47	20	140
CHVC 186+19−114	07 16.9	+31 46	0.°9 × 0.°6 @ −20°	1.03	20	177
CHVC 358+12−137	16 55.3	−23 33	0.°8 × 0.°8	0.56	19	112

Group. The proximity to M 31 has previously led to speculation regarding a possible association with that galaxy (Davies 1975). CHVC 186+19−114 has recently been mapped with the Arecibo telescope with a spatial resolution of 3′ (Burton et al. 2001).

3. Observations

Observations of the five CHVC fields were obtained with the WSRT during July and August, 1999. The CHVCs at southern declinations could not be observed with complete 12–hour tracks due to elevation limitations. Although complete 12–hour tracks were scheduled for the sources at northern declinations these were not completely successful. The actual hour–angle coverage obtained for each source is indicated in Table 2, together with the nominal east-west separation of telescopes RT9 and RTA. Program observations were preceded and followed by observations of one of the calibration sources 3C48, 3C286, or 1938−155. At the time of the observations all 14 telescopes of the array were equipped with the upgraded MFFE receivers. These receivers have a system temperature of about 27 K in the 1150 to 1850 MHz band. The correlator was configured to provide 256 uniformly weighted spectral channels in two linear polarizations across 2.5 MHz centered on the V_{LSR} velocity of each source. The effective velocity resolution was 1.2 times the channel spacing, which was 0.5 km s^{-1} for CHVC 148−82−258 and 1.0 km s^{-1} for the other sources.

Standard gain and bandpass calibrations were carried out after editing the data for incidental interference and shadowing. Self–calibration utilizing continuum sources in the target fields has been used, where necessary, to further calibrate the gains. This was particularly required for the sources at negative declinations, which were observed at relatively low elevations. An image made from the average of the emission–free spectral channels from each field provided a CLEAN component model of the continuum emission. This model was subtracted directly from the visibility data. The block of spectral channels containing line emission was imaged with a visibility–based CLEAN deconvolution proceeding down to a flux level of twice the rms noise level. Uniform weighting of the visibility data was employed together with a Gaussian taper decreasing to 30% amplitude at a projected baseline of 1.25 kλ. The corresponding spatial resolution was about 60 arcsec. The velocity axis has been smoothed with a Gaussian with a *FWHM* of 1 km s^{-1} for CHVC 148−82−258, and of 2 km s^{-1} for the other sources. Given the low observed brightness of the sources, the application of the spatial taper and velocity smoothing were required to get a usefully high signal–to–noise ratio. In a few cases, some residual continuum emission was still present in the data cubes. In those cases, several spectral channels from both edges of the cube were averaged together and subtracted from the entire cube.

The typical rms noise level in the deconvolved WSRT cubes listed in Table 2 was between 2.0 and 4.0 mJy per beam per spectral channel, with the northern–declination cubes generally superior in this respect to the southern ones. The corresponding brightness sensitivities are also listed in Table 2. (Flux per beam and brightness temperature are related as usual by $S = 2k_B T_B \Omega_B / \lambda^2$, or $S_{mJy/Beam} = 0.65\ \Omega_{as} T_B / \lambda^2_{cm}$, where Ω_{as} is the beam area in arcsec^2.) Expressed as an optically thin HI column density, the sensitivity corresponds to about 0.4×10^{18} cm^{-2}, for emission which fills the beam and which extends over a single velocity channel of 2 km s^{-1} width. Since diffuse H I in the halo component has a minimum observed linewidth of about 24 km s^{-1} *FWHM*, the more relevant column–density sensitivity is a factor of $\sqrt{12}$ higher over this larger linewidth.

Moment images of zero, first, and second order were generated from each cube, after employing a blanking criterion for inclusion of each pixel in the weighted sum. This involved demanding a brightness in excess of about 2σ after smoothing the cube by an additional factor of three, both spatially and in velocity. Images of integrated emission were corrected for the primary–beam response of the WSRT instrument, which is well approximated, at 1420 MHz, by a circular Gaussian with 2110 arcsec *FWHM*.

By their nature, interferometers are insensitive to diffuse emission more extended than about $1/B_{min}$ radians, for a minimum baseline, B_{min}, expressed in wavelengths. The ratios between the fluxes as measured with single–dish total–power observations and the WSRT data clearly show that not all the flux is recovered; the percentage of recovered flux is indicated in the last column of Table 2. In general, only the narrow linewidth cores are detected in the WSRT data. To compensate for this shortcoming, the WSRT data are compared here with total–power data for the individual sources. For CHVC 186+19−114, the total–power data are those obtained from Arecibo observations made by Burton et al. (2001); for CHVC 148−82−258 and CHVC 358+12−137, HIPASS data were used, as both of these sources lie in the zone of overlap between the LDS and the HIPASS material and were also entered in the CHVC

Table 2. Parameters of the WSRT observations and some measured CHVC properties.

Object	HA range	$B_{\rm min}$	resolution	RMS	RMS	detected flux	percentage
CHVC *lll* ± *bb* ± *vvv*	(h→h)	(m)	($a'' \times b''$ @ PA° × km s^{-1})	(mJy/beam)	(K)	(Jy km s^{-1})	detected
CHVC 120−20−443	−6 → +1	63	198 × 82 @ − 30°× 2.1	2.7	0.10	8	8%
CHVC 129+15−295	−4 → +6	54	135 × 98 @ − 19°× 2.1	2.8	0.13	17	14%
CHVC 148−82−258	−6 → +3.5	48	514 × 92 @ − 3°× 1.0	4.4	0.06	6	4%
CHVC 186+19−114	−3 → +2.5	54	130 × 87 @ + 28°× 2.1	3.1	0.17	28	16%
CHVC 358+12−137	−2 → +2	96	468 × 72 @ − 19°× 2.1	3.3	0.06	4	4%

catalog of Putman et al. (2002); for CHVC 120−20−443, observations were made using the 140–foot telescope of the NRAO in Green Bank; for CHVC 129+15−295, only LDS data were used. The Arecibo observations have a spatial resolution of about 3′; the HIPASS observations (Barnes et al. 2001), fully Nyquist sampled with the 64–m Parkes telescope, have a spatial resolution of 15.′5 *FWHM*; the Green Bank 140–foot telescope had a beam size of 21′ *FWHM*; the Dwingeloo 25–m telescope had a beam size of 36′ *FWHM*.

The observations made with the NRAO 140–foot telescope of CHVC 120−20−443 were carried out during two runs, in November/December, 1996, and in September, 1997, as part of a larger program tracing anomalous–velocity H I within some 10 degrees of M 31. The observations were made in frequency–switching mode (switching up 5 MHz), with a bandwidth of 5 MHz. Spectra were taken on a 10–arcminute grid; the *FWHM* beam of the 140–foot antenna is 21′ at λ21 cm. The spectral coverage extended from $V_{\rm LSR} = -700$ km s^{-1} to +300 km s^{-1}. On–source integration times were 40 s. Conversion from antenna temperatures to brightness temperatures followed from regular observations of the primary standard field S8 and use of the conversion factors of Williams (1973).

4. High–resolution images

4.1. CHVC 120−20−443

Discovered by Davies (1975), CHVC 120−20−443 is especially interesting given its projected proximity to M 31 and its extreme velocity. The object is centered only about 2° north of the M 31 nucleus and lies directly adjacent to the north–eastern disk of that system, as shown in Fig. 1, which displays integrated H I data obtained with the NRAO 140–foot telescope. The moment map on the left side of this figure represents $N_{\rm HI}$ in the velocity range $-490 < V_{\rm LSR} < -160$ km s^{-1}, and so includes much of the full extent of M 31; the moment map on the right shows $N_{\rm HI}$ from the restricted range of velocities, $-470 < V_{\rm LSR} < -420$ km s^{-1}, over which the CHVC itself contributes H I emission. There is no sign of a bridge of H I connecting the CHVC and M 31 at the sensitivity of these data, but there are suggestions of a physical influence of M 31 on the cloud in other aspects of the observations which we discuss below.

An overview of the WSRT results is given in Fig. 2. The highest column densities in this CHVC are concentrated in a semi–circular rim along the eastern periphery – i.e. in the direction of the M 31 disk. The object is characterized by rather disjoint internal kinematics. Mean line–of–sight velocities vary over a range of some 30 km s^{-1}, but do not do so smoothly. The line–of–sight velocities are almost bi–modally distributed, with a more circularly symmetric component near $V_{\rm LSR} = -455$ km s^{-1}, in addition to the eastern rim feature centered near −440 km s^{-1}. The eastern rim of this object is also remarkable for the broad velocity widths seen there. Velocity dispersions as high as 10 km s^{-1} are observed. The broad linewidths of this feature can be seen in the individual spectra of Fig. 3; Gaussian fits to the spectra are listed in Table 3. None of the other objects presented here show comparably broad linewidths in the cool cores detected with synthesis imaging. In the earlier WSRT sample of Braun & Burton (2000) such broad linewidths were only seen in systems that showed indications of line–of–sight overlap of multiple distinct velocity systems. In this case, however, the broad linewidths appear to be intrinsic to the feature, or perhaps related to the bimodal velocity distribution noted above.

The high–resolution WSRT channel maps are overlaid in Fig. 4 on the total–power data from the 140–foot telescope. The diffuse H I detected in the total–power data is significantly offset toward the southeast from the core components seen at high resolution.

4.2. CHVC 129+15−295

The extended environment of CHVC 129+15−295 is illustrated in Fig. 5, which shows on the left an image of velocity–integrated H I extracted from the Leiden/Dwingeloo survey. The CHVC is completely isolated in position as well as in velocity, down to the 3σ noise limit of the LDS, corresponding to less than 1.5×10^{18} cm^{-2}. This object corresponds to entry #231 in the general catalog of Wakker & van Woerden (1991), to entry #31 in CHVC catalog of Braun & Burton (1999), and to #72 in the CHVC catalog of de Heij et al. (2002a). The nearest high–velocity cloud complexes, as cataloged by Wakker & van Woerden (1991), are Complex A, which extends to (l = 130°, b = +22°), and Complex H located around (l = 130°, b = +5°). But the velocity differences with respect to both of these complexes amount to more than 70 km s^{-1}: a physically–relevant relation of the CHVC to either one of the complexes is not demonstrated. The WSRT moment images for this field are shown in Fig. 6. The cloud core has the shape of an inverted V–shaped filament which is brighter on the west side than on the east. Peak column densities reach about 5×10^{19} cm^{-2}. The WSRT moment images show no significant variation in the mean velocity or in the velocity width.

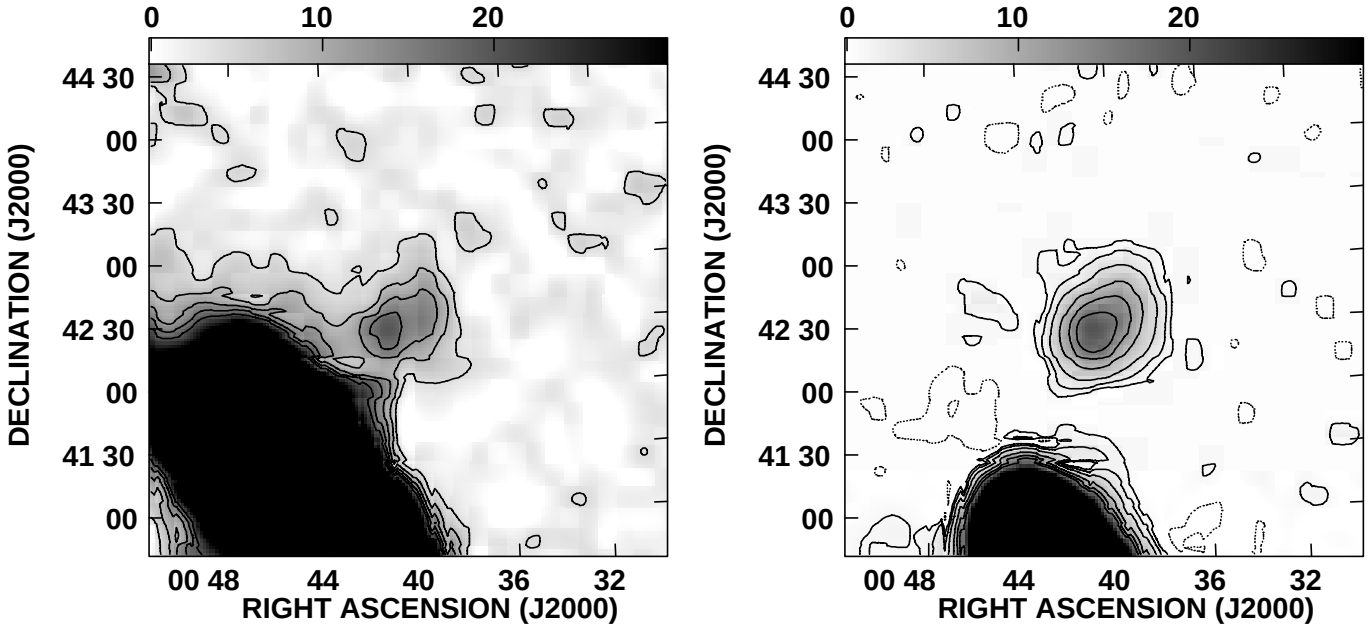

Fig. 1. Two images of integrated H I emission illustrating the environment of Davies' cloud, CHVC 120−20−443. *Left*: H I emission integrated over the velocity interval $-490 < V_{\rm LSR} < -160$ km s^{-1}, a range which encompasses most of the emission from M 31. Contours of H I column density are drawn at 4, 8, 12, 16, and 20×10^{18} cm^{-2}. The grey–scale bar in both panels is labelled in units of 10^{18} cm^{-2}. The disk of M 31 is directly adjacent to the CHVC although offset in velocity. *Right*: H I emission integrated over the velocity interval $-470 < V_{\rm LSR} < -420$ km s^{-1}, corresponding to the total velocity extent of the CHVC. Contours of $N_{\rm HI}$ are drawn at levels of −1, 1, 2, 4, 8, 12, and 16×10^{18} cm^{-2}. No bridge of emission is evident at these velocities between the CHVC and M 31, although the centroid of the cloud emission is suggestively skewed towards M 31.

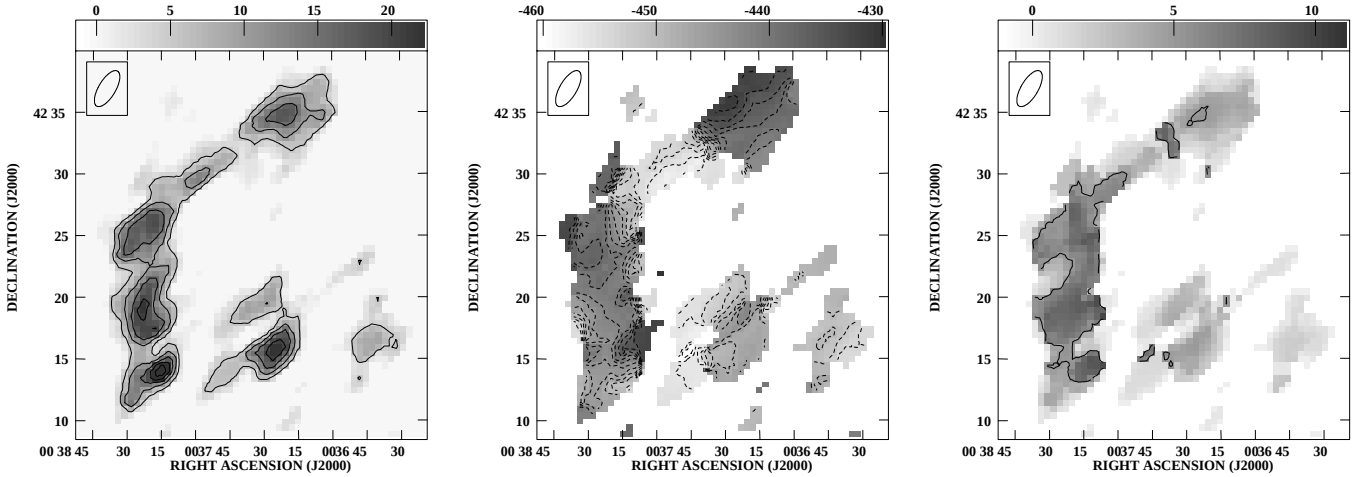

Fig. 2. CHVC 120−20−443 as imaged with the WSRT at resolutions of 2×1 arcmin and 2 km s^{-1}. *Left*: Integrated H I with contours drawn at 2.5, 5.0, 7.5, and 10.0 K km s^{-1}, and a linear grey–scale extending from −1 to 12 K km s^{-1}. *Middle*: Intensity–weighted line–of–sight velocity, $V_{\rm LSR}$, with contours drawn at −458, −456, ..., −432 km s^{-1}, and a linear grey–scale extending from −460 to −430 km s^{-1}. *Right*: Distribution of the intensity–weighted velocity dispersion, with a linear grey–scale extending from 0 to 11 km s^{-1}. The contour corresponds to a dispersion of 5 km s^{-1}.

Representative WSRT spectra, shown on the righthand side of Fig. 5, are all centered near −305 km s^{-1}, with a *FWHM* of about 5 km s^{-1}. The results of one–component Gaussian fits to the spectra are tabulated in Table 3. The maximum velocity dispersion nowhere exceeds 4 km s^{-1}, and is typically much less. The narrow widths imply both that the temperatures are low and that the object is kinematically quiet.

4.3. CHVC 186+19−114

CHVC 186+19−114, with a peak brightness temperature of 1.1 K at half-degree angular resolution, is one of the brighter objects in the de Heij et al. (2002a) catalog of CHVCs. This object corresponds to entry #215 in the general catalog of Wakker & van Woerden (1991), to entry #44 in CHVC catalog of Braun & Burton (1999), and to #92 in the catalog

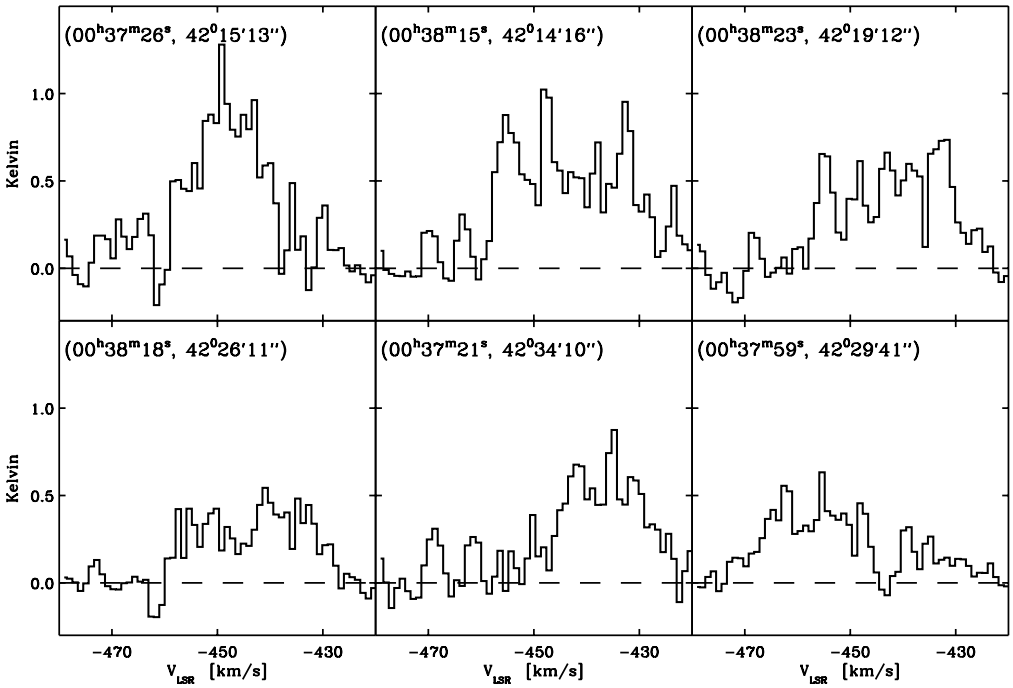

Fig. 3. Brightness temperature WSRT spectra of CHVC 120−20−443 at the indicated positions.

of de Heij et al. A velocity–integrated intensity map, based on the Leiden/Dwingeloo survey and shown in lefthand panel of Fig. 7, does not reveal much detail, but illustrates well the isolated nature of this source. An overview of the WSRT data for CHVC 186+19−114 is given in Fig. 8. The velocity–integrated map shows an ellipsoidal structure with the highest detected column densities along both the eastern and northern edges as well as a single high–contrast clump at (α, δ = ($07^{\rm h}17^{\rm m}18^{\rm s}$, 31°33′36″), which reaches a peak column density of about 1.5×10^{20} cm^{-2}.

The core/halo morphology of this CHVC is seen by comparing the Arecibo observations of Burton et al. (2001) with the current WSRT material. An overlay of the Arecibo and WSRT observations, which illustrates cloud structures down to a spatial resolution of about 1×2 arcmin, is shown in Fig. 9. Although there is no obvious large–scale gradient apparent in the WSRT velocity field, the sequence of Arecibo channel maps shown in Fig. 9 does indicate a clear gradient amounting to some 20 km s^{-1} over 50 arcmin, extending from −125 km s^{-1} in the northeast to −105 km s^{-1} in the southwest. The highest velocity dispersions are seen toward the clump noted above. The doubly–peaked spectrum in this direction, shown on the righthand side of Fig. 7, is suggestive of velocity splitting of about 7 km s^{-1}. The parameters of the best–fitting combination of two Gaussian components are listed in Table 3. This decomposition consists of a relatively narrow component centered at −122 km s^{-1}, and a somewhat broader component centered at −115 km s^{-1}. Gaussian decompositions are notoriously non–unique under many common circumstances, and often completely unphysical, so no undue significance should be attached to these specific values. A comparison with the Arecibo spectra, indicated by the dashed lines in the lefthand panel of Fig. 7, shows that the Arecibo data can be described by a single broad component centered at an intermediate velocity, −118 km s^{-1}, with no enhancement at −122 km s^{-1}. A second compact clump seen in the WSRT data at (α, δ) = ($07^{\rm h}17^{\rm m}25^{\rm s}$, 31°43′12″) displays a similar effect. The narrow WSRT profile is centered at −122 km s^{-1}, while the wider Arecibo profile is centered at −119 km s^{-1}. The effects of different angular resolution and (lack of) sensitivity to the most diffuse structures are seen to produce substantial differences in the spectra.

4.4. CHVC 148−82−258 and CHVC 358+12−137

These two compact high–velocity clouds were discovered by Braun & Burton (1999) in the LDS material, and enter their catalog as #36 and #66, respectively. CHVC 148−82−258 also corresponds to entry #67 in the CHVC catalog of de Heij (2002a) and to entry #1545 in the Putman et al. (2002) HIPASS catalog. CHVC 358+12−137 corresponds to #109 in de Heij et al., and to #2165 in Putman et al. The southerly declinations of these two sources limited the image quality that could be obtained with the WSRT array (which is sited at 54° north geographic latitude). The limited (U,V) coverage listed in Table 2 resulted in a highly elongated synthesized beam, of about $1' \times 8'$, and a high sidelobe level. Even after deconvolution, the resulting image fidelity was not high, as judged by the non–Gaussian character of the deconvolution residuals.

The WSRT results for these two objects are summarized in Figs. 10 and 11, respectively. The figures show the WSRT integrated H I contours overlaid on the HIPASS total–power data. Only a few percent of the total flux has been detected by the interferometer in these objects, as indicated in Table 2. Peak column densities are only about 1×10^{19} cm^{-2}. The locations

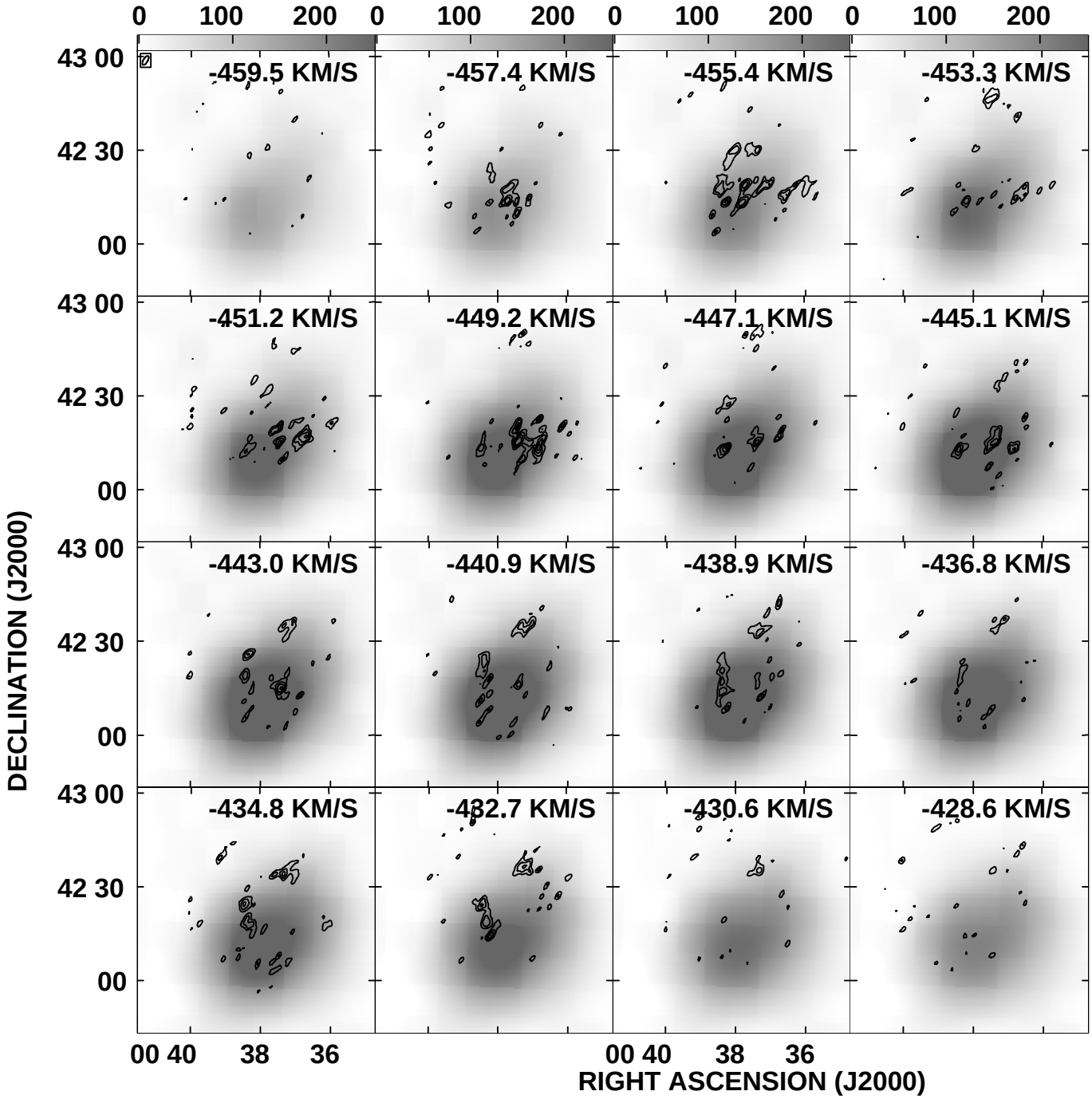

Fig. 4. Overlay of WSRT and Green Bank 140–foot channel maps for CHVC 120−20−443. The WSRT contours are drawn at 0.4, 0.6, 0.8, and 1.0 K; the data from the 140–foot telescope are represented as a grey–scale extending from 0 to 250 milli–Kelvin. Only about 8% of the total flux measured in the tota–power observations is recovered by the interferometer.

of the compact structures detected in the synthesis data are not coincident with the locations of the brightest regions of the 15′ resolution HIPASS data. Representative spectra of both clouds are shown in the righthand panels of Figs. 10 and 11, respectively. The results of Gaussians fits to the spectra are given in Table 3.

The emission detected by the WSRT in CHVC 148−82−258 is concentrated in a single elongated clump, centered near −272 km s^{-1}. Small differences in the centroid velocity, of about 1 km s^{-1}, are seen at the various positions.

The WSRT observations of CHVC 358+12−137 show four major clumps, with centroid velocities ranging from −144 to −138 km s^{-1}. The most easterly of these clumps, at (α, δ) = ($16^{\rm h}56^{\rm m}09^{\rm s}$, 23°32′53″), shows some indication for line–splitting, although the signal–to–noise ratio is low. At face value this splitting amounts to some 10 km s^{-1}, as listed in Table 3.

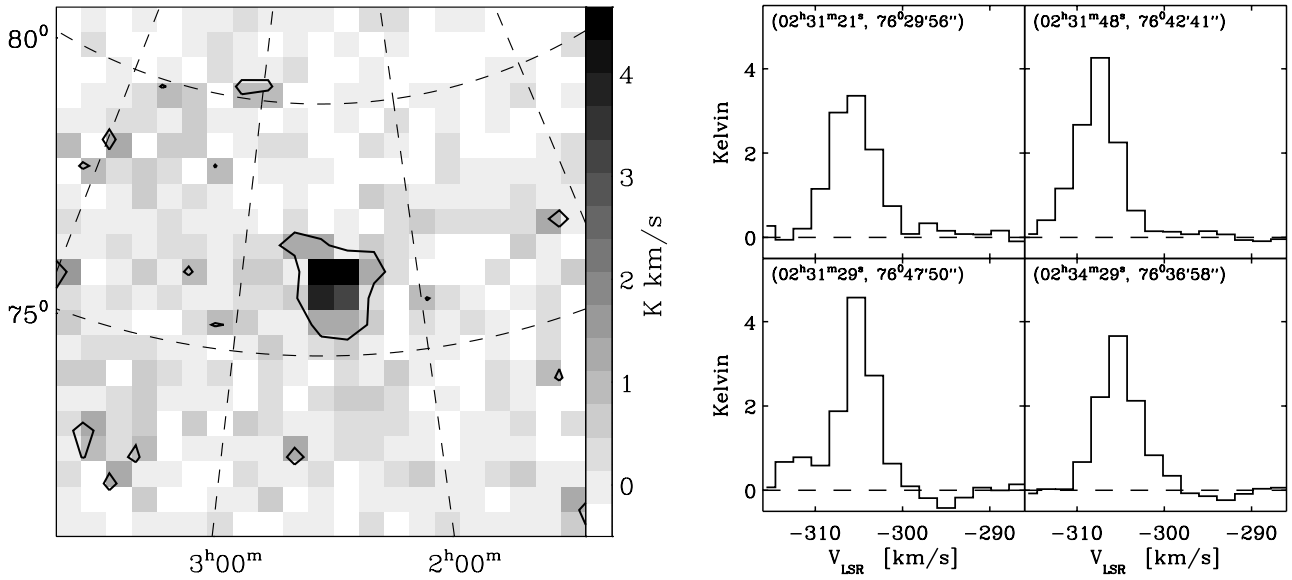

Fig. 5. *Left*: Velocity–integrated intensity map of CHVC 129+15−295 derived from the Leiden/Dwingeloo survey. The range of integration extends from the average velocity minus the *FWHM* to the average velocity plus the *FWHM*. The single contour is drawn at $N_{\rm HI} = 1.5 \times 10^{18}$ cm^{-2}. *Right*: Brightness temperature spectra of CHVC 129+15−295, measured with the WSRT at the indicated positions.

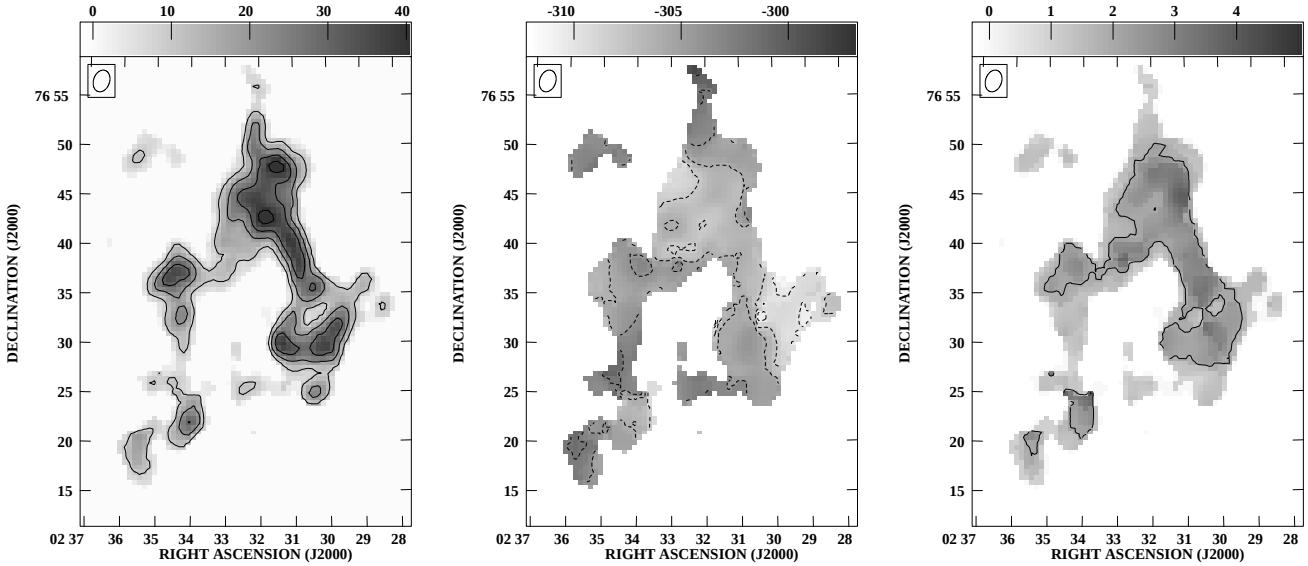

Fig. 6. CHVC 129+15−295 at 2 × 1 arcmin and 2 km s^{-1} resolution. *Left*: Apparent integrated HI in K km s^{-1} with contours at 5, 10, 15, 20 K km s^{-1} and a linear grey–scale extending from −1 to 25 K km s^{-1}. *Middle*: Intensity–weighted line–of–sight velocity, $V_{\rm LSR}$, with contours drawn at −312, −310, ..., −298 km s^{-1} and a linear grey–scale extending from −312 to −297 km s^{-1}. *Right*: Distribution of the intensity–weighted velocity dispersion, with a linear grey–scale extending from 0 to 5 km s^{-1}. The contour corresponds to a dispersion of 2 km s^{-1}.

5. Discussion

5.1. Cool and warm neutral media

Wolfire et al. (1995), following on the earlier treatments by Field et al. (1969) and Draine (1978), have shown that diffuse H I clouds in thermodynamic equilibrium might have a two–phase temperature structure. The two components, a cool one (CNM) with temperatures around 100 K, and a warm one (WNM) with temperatures around 10^4 K, can coexist in pressure equilibrium for thermal pressures, P/k_B, in the range of about 100–2000 cm^{-3} K. The calculations presented in Wolfire et al. (1995) have been supplemented with new ones appropriate for a low metallicity population of CHVCs residing at significant distances in the Local Group environment. The results of these new calculations are shown in Fig. 13 of Braun & Burton (2000), where equilibrium solutions are given for clouds with a shielding column density of 1 and 10×10^{19} cm^{-2}, a metallicity of 0.1 solar, and a dust–to–gas mass ratio of 0.1 times the value in the solar neighborhood.

The velocity *FWHM* of H I clouds with kinetic temperatures of 100 K and 10^4 K are 2.4 km s^{-1} and 24 km s^{-1}, respectively. As shown in Table 3, the values observed in the

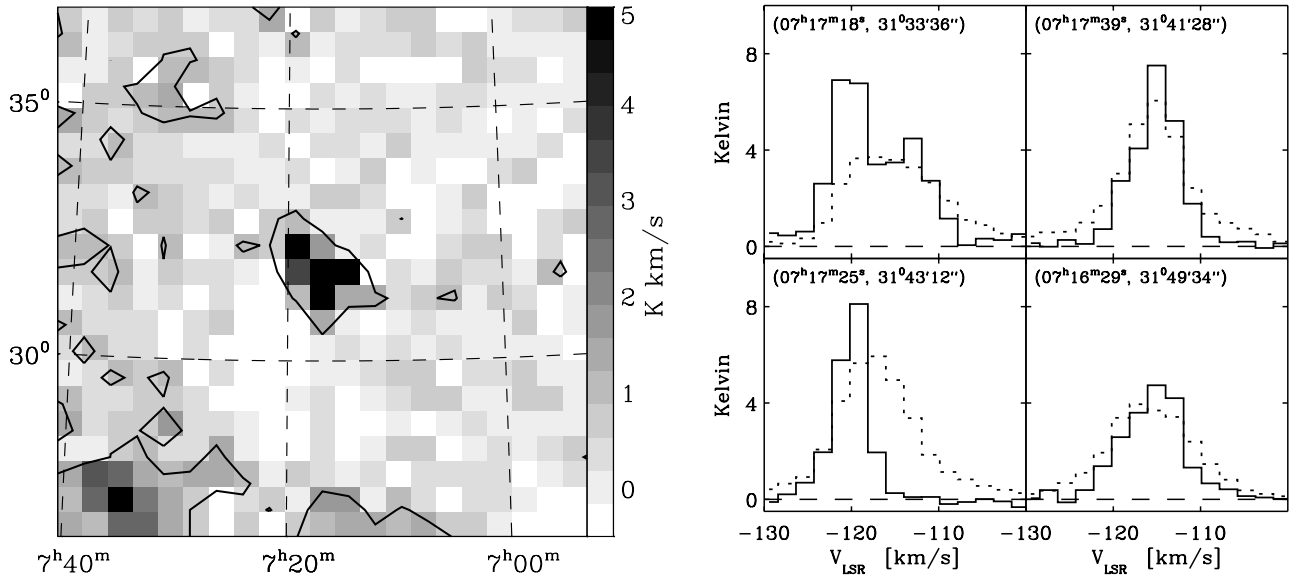

Fig. 7. *Left*: Velocity–integrated intensity map of CHVC 186+19−114 derived from the Leiden/Dwingeloo survey. The range of integration extends from the average velocity minus the *FWHM* to the average velocity plus the *FWHM*. The single contour is drawn at $N_{\rm HI} = 1.5 \times 10^{18}$ cm^{-2}. *Right*: Brightness temperature spectra of CHVC 186+19−114 at the indicated positions. Solid lines refer to spectra from the WSRT, dashed lines to spectra from the Arecibo telescope.

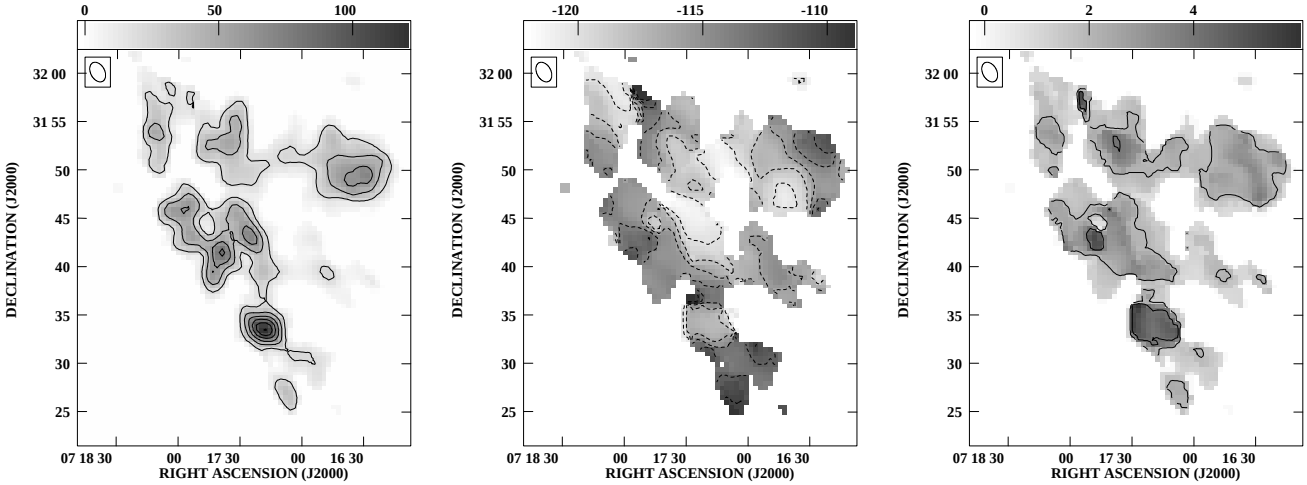

Fig. 8. CHVC 186+19−114 as observed with the WSRT at a spatial resolution of 2 × 1 arcmin and a kinematic resolution of 2 km s^{-1}. *Left*: Apparent integrated HI in units of K km s^{-1}, with contours drawn at 10, 20, ..., 80 K km s^{-1}, and with a linear grey–scale extending from −1 to 68 K km s^{-1}. *Middle*: Intensity–weighted line–of–sight velocity, $V_{\rm LSR}$, with contours at −120, −118, ..., −110 km s^{-1} and linear grey–scale extending from −122 to −109 km s^{-1}. *Right*: Distribution of the intensity–weighted velocity dispersion, with a linear grey–scale extending from 0 to 6 km s^{-1}. The contours correspond to dispersions of 2 and 4 km s^{-1}, respectively.

high–colum–density cores detected in the WSRT observations of our sample vary between *FWHM* of about 4 and 30 km s^{-1}. No new example of ultra–narrrow H I lines was detected, such as the 2 km s^{-1} *FWHM* features seen in CHVC 125+41−207 by Braun & Burton (2000). The median linewidth of the material being discussed here amounts to about 6 km s^{-1} *FWHM*, a width comparable to that seen at high resolution in both HVC and CHVC studies (Wakker & Schwarz 1991; Braun & Burton 2000) as well as in nearby external spiral galaxies (Braun 1997). This is somewhat broader than expected for the thermal linewidth of a 100 K gas, suggesting that either some form of ordered or random internal motions are present, or that the available resolution does not adequately account for line–of–sight blending of separate components. The alternative, namely that the typical kinetic temperature is actually about 650 K, seems to be ruled out by observations of H I absorption in HVCs, as well as in the Galaxy and external galaxies, which reveal spin temperatures of 50 to 175 K in all cases (see Wakker et al. 1991; Braun & Walterbos 1992; Braun 1995).

The large velocity widths, of 25 to 30 km s^{-1} *FWHM*, found in the condensations along the eastern rim of CHVC 120−20−443 are difficult to interpret in this context. Of the thirteen CHVCs which have currently been subjected to arcmin resolution synthesis imaging, only one other instance of broad CNM linewidths has been observed, namely in

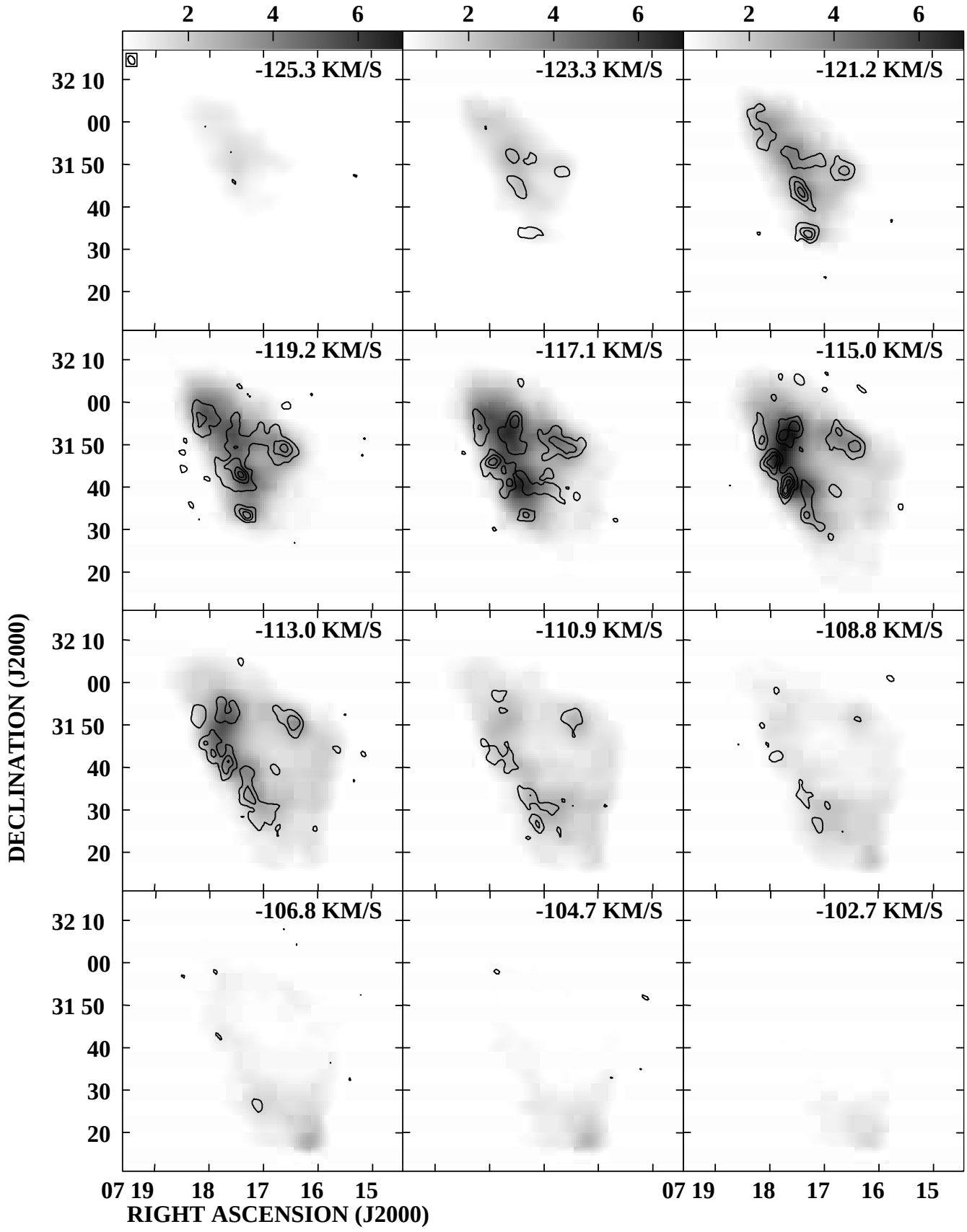

Fig. 9. Overlay of WSRT and Arecibo intensity data for CHVC 186+19−114. The WSRT intensities detected at a resolution of 1×2 arcmin are indicated by contours drawn at 1, 3, 5, 7 K. The Arecibo data at 3 arcmin resolution are indicated by the grey–scale images, with the scale given by the color bar in units of Kelvin.

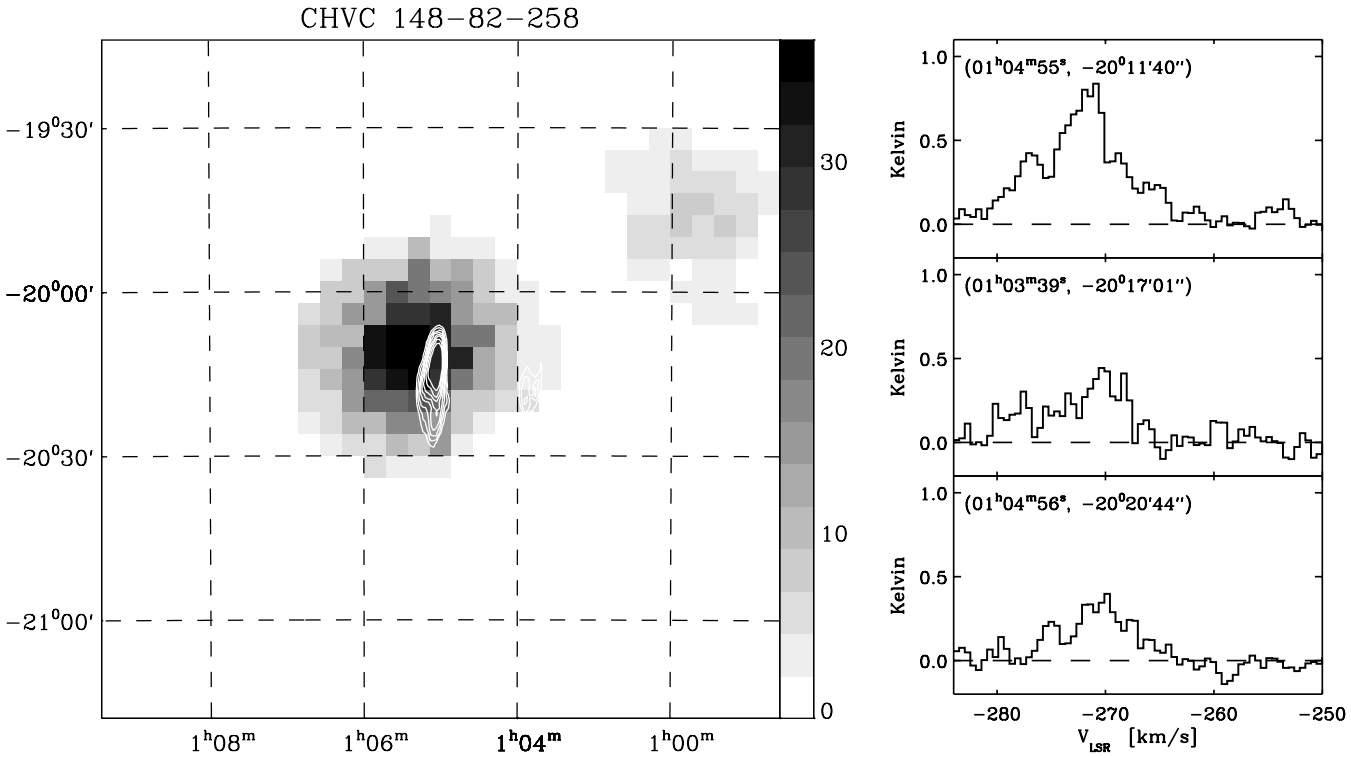

Fig. 10. *Left*: Overlay of WSRT and HIPASS $N_{\rm HI}$ data for CHVC 148+82−258. The WSRT detected H I column density at 1.5×8.5 arcmin resolution is indicated by contours which are drawn at 2, 3, $4 \ldots 9 \times 10^{18}$ cm^{-2}. The 15.5 arcmin HIPASS data are indicated by the grey–scale images in units of 10^{18} cm^{-2}. *Right*: Brightness temperature spectra of CHVC 148−82−258, measured with the WSRT at the indicated positions.

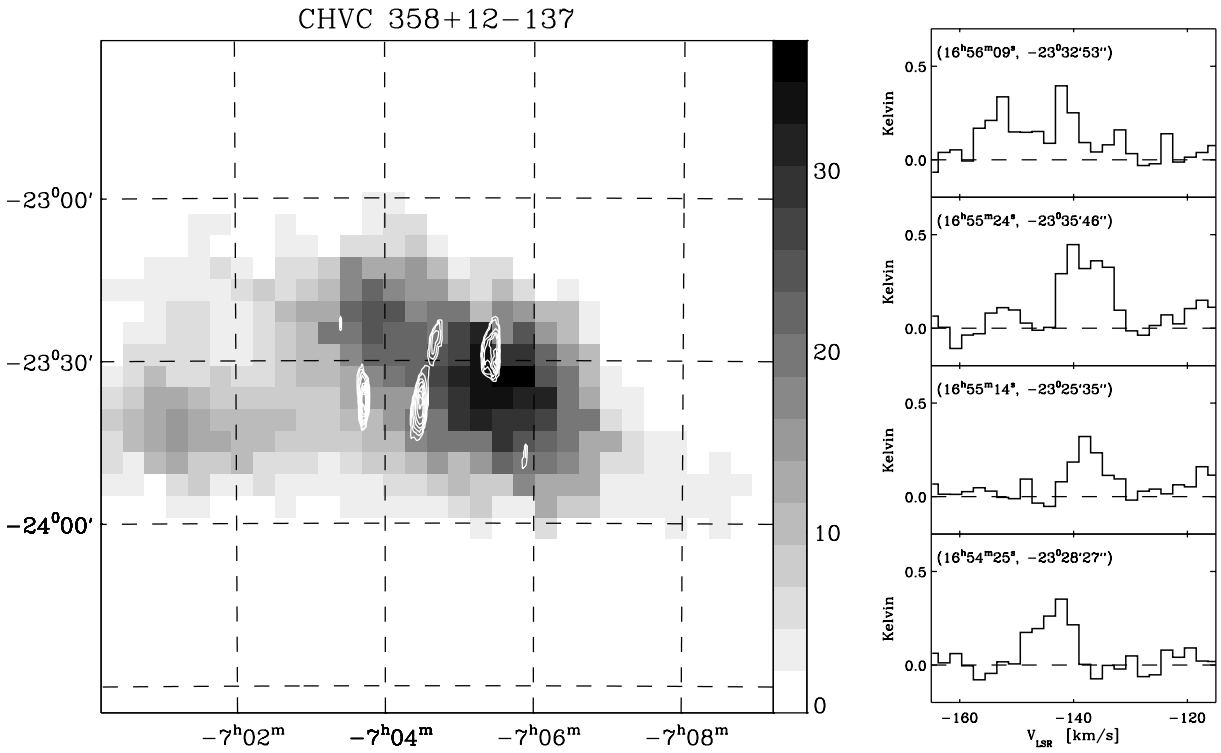

Fig. 11. *Left*: Overlay of WSRT and HIPASS $N_{\rm HI}$ data for CHVC 358+12−137. The WSRT detected H I column density at 1×8 arcmin resolution is indicated by contours which are drawn at 2, 3, $4 \ldots 9 \times 10^{18}$ cm^{-2}. The 15.5 arcmin HIPASS data are indicated by the grey–scale images in units of 10^{18} cm^{-2}. *Right*: Brightness temperature spectra of CHVC 358+12−137, measured with the WSRT at the indicated positions.

Table 3. Gaussian fits to the brightness temperature spectra shown in the figures.

RA (2000)	Dec (2000)	$T_{\rm peak}$ (K)	$V_{\rm LSR}$ (km s^{-1})	*FWHM* (km s^{-1})
CHVC 120−20−443				
$00^{\rm h}37^{\rm m}26^{\rm s}$	+42°15′13″	0.94	−448	16.0
$00^{\rm h}38^{\rm m}15^{\rm s}$	+42°14′16″	0.67	−444	29.7
$00^{\rm h}38^{\rm m}23^{\rm s}$	+42°19′12″	0.56	−441	25.8
$00^{\rm h}38^{\rm m}18^{\rm s}$	+42°26′11″	0.40	−442	24.1
$00^{\rm h}37^{\rm m}21^{\rm s}$	+42°34′10″	0.64	−437	18.5
$00^{\rm h}37^{\rm m}59^{\rm s}$	+42°29′41″	0.41	−456	25.0
CHVC 129+15−295				
$02^{\rm h}31^{\rm m}21^{\rm s}$	+76°29′56″	3.5	−305	5.8
$02^{\rm h}30^{\rm m}09^{\rm s}$	+76°29′42″	2.7	−306	7.3
$02^{\rm h}31^{\rm m}48^{\rm s}$	+76°41′41″	4.1	−308	5.3
$02^{\rm h}31^{\rm m}29^{\rm s}$	+76°47′50″	4.5	−305	4.4
$02^{\rm h}34^{\rm m}29^{\rm s}$	+76°36′58″	3.5	−305	5.3
CHVC 148−82−258				
$01^{\rm h}04^{\rm m}55^{\rm s}$	−20°11′40″	0.63	−272	9.8
$01^{\rm h}04^{\rm m}56^{\rm s}$	−20°20′44″	0.31	−271	7.7
$01^{\rm h}03^{\rm m}39^{\rm s}$	−20°17′01″	0.30	−272	10.2
CHVC 186+19−114, Arecibo				
$07^{\rm h}17^{\rm m}18^{\rm s}$	+31°33′36″	3.9	−118	13.3
$07^{\rm h}17^{\rm m}39^{\rm s}$	+31°41′28″	5.6	−117	9.4
$07^{\rm h}17^{\rm m}25^{\rm s}$	+31°43′12″	5.9	−119	10.4
$07^{\rm h}16^{\rm m}29^{\rm s}$	+31°49′34″	4.0	−118	11.8
$07^{\rm h}18^{\rm m}11^{\rm s}$	+31°53′56″	3.6	−119	10.4
CHVC 186+19−114, WSRT				
$07^{\rm h}17^{\rm m}18^{\rm s}$	+31°33′36″	7.6	−122	4.8
		4.4	−115	5.8
$07^{\rm h}17^{\rm m}39^{\rm s}$	+31°41′28″	7.0	−117	6.3
$07^{\rm h}17^{\rm m}25^{\rm s}$	+31°43′12″	8.4	−122	3.9
$07^{\rm h}16^{\rm m}29^{\rm s}$	+31°49′34″	4.7	−118	7.7
$07^{\rm h}18^{\rm m}11^{\rm s}$	+31°53′56″	3.5	−119	7.7
CHVC 358+12−137				
$16^{\rm h}56^{\rm m}09^{\rm s}$	−23°32′53″	0.27	−152	7.7
		0.40	−142	3.9
$16^{\rm h}55^{\rm m}24^{\rm s}$	−23°35′46″	0.43	−138	8.7
$16^{\rm h}55^{\rm m}14^{\rm s}$	−23°25′35″	0.31	−138	6.3
$16^{\rm h}54^{\rm m}25^{\rm s}$	−23°28′27″	0.33	−143	7.3

CHVC 110.6−07.0−466 (Hulsbosch's cloud) as imaged by Wakker & Schwarz (1991). Several other cases of broad widths are not relevant in this context, because they could be unambiguously attributed to line–of–sight overlap of components at different velocities. As noted above in Sect. 4, it is not clear whether the linewidths in this feature are intrinsic or whether the velocity field becomes systematically double–valued at this location. We will return to this issue in a following subsection.

In general, it seems clear that it is predominantly the CNM which is detected in the WSRT images for objects of 0.°5 or more in size. The smoothly distributed WNM can not be readily detected in the synthesis data. The fractional flux of CNM in the five objects studied here varies from about 4% to 16%. This fraction varied from less than 1% to more than 50% in the Braun & Burton (2000) sample, which spanned a larger range of source properties. It is noteworthy that in all CHVCs studied to date with high spatial resolution there has been at least a marginal detection of the CNM. Every one of the thirteen CHVCs studied to date has at least one local peak in the CNM column density which exceeds about 10^{19} cm^{-2} when observed with arcmin resolution. The accompanying diffuse WNM halo reaches comparable peak column densities, of about 1 or 2×10^{19} cm^{-2}, external to these peaks (Burton et al. 2001). It is conceivable that a WNM halo column density of 1 or 2×10^{19} cm^{-2} is a prerequisite for the long–term survival of these sources. It may be no coincidence that Maloney (1993) and Corbelli & Salpeter (1993) estimated this value as the critical column density needed to prevent complete ionization of the H I when exposed to the estimated extragalactic ionizing radiation field relevant for free–floating objects in the Local Group.

5.2. Velocity offsets of cool cores and warm halos

In the case of CHVC 186+19−114, it was possible to make a detailed comparison of line profiles as measured in CNM cores using the WSRT with the sum of the CNM and WNM emission detected in the 3–arcmin beam of the Arecibo telescope. The CNM spectra show narrower intrinsic widths as well as some local differences in the centroid velocity, while the Arecibo spectra display broad–linewidth tails (consistent with a 10^4 K thermal component) and much less dramatic variation in the profile shape and centroid. Given the dominant role of the WNM, accounting for about 84% of the total H I flux in this source, these differences are not surprising. Although the WSRT and Arecibo velocity centroids often agree, there are a few isolated locations where the CNM component is offset from the total H I centroid by a few km s^{-1}. If a systematic velocity offset had been apparent between the WSRT and Arecibo spectra, it might have been an indication for an external perturbation of the source.

Brüns et al. (2001), who have observed the interesting object CHVC 125+41−207 with the 100–m Effelsberg telescope, argue that there is a systematic velocity offset between a narrow and broad component of the H I emission in that source. Their conclusion is based on Gaussian decompositions of the slightly asymmetric line profiles in the Effelsberg spectra. The decompositions result in two components; one of about 5 km s^{-1} and the other of 12 km s^{-1} *FWHM*. It is difficult to assess the physical relevance of these decomposition results, since at large distances from the CHVC centroid a single Gaussian of about 20 km s^{-1} is found to suffice in fitting the Effelsberg spectra well, while within the CHVC centroid, the WSRT data of Braun & Burton (2000) for this object show non–Gaussian CNM line profiles of only 2 to 4 km s^{-1} *FWHM*. Given the intrinsic non–uniqueness of Gaussian decomposition when applied to non–Gaussian line profiles, it seems questionable whether the 5 and 12 km s^{-1} *FWHM* Gaussian–fit components refer to physical systems at all.

If a systematic offset of the CNM and WNM velocities were present, then this might indicate that the halo kinematics is perturbed by an external force, which has not yet perturbed the central core of the cloud. The gravitational tidal field of either the Galaxy or M 31 is a candidate for such a differential force. Another possibility is the ram–pressure exerted on the cloud

as it moves through an external medium. Given the substantial differences in sound–crossing times of the cores relative to the halo, a significant time delay in the response might result.

5.3. The particular interest of CHVC 120−20−443

In his 1975 paper, Davies considered two possible interpretations of this cloud. Given its proximity to M 31 on the sky, it might be located at a comparable distance, with a projected separation of only 18 kpc. Since peak column densities are only a few times 10^{19} cm^{-2}, internal star formation is unlikely: our non–detection of stars in Palomar Sky Survey prints is no surprise. With only the visible baryonic mass, Davies concluded that the cloud is not gravitationally bound, and will double its size on a time scale of 2.4×10^8 years. As an alternative possibility he considered that the cloud might be related in some way to the Magellanic Stream. The closest approach of this feature to portions of the Stream is, however, about 30° in angle and about 65 km s^{-1} in velocity, making such an association tenuous at best. If the cloud were a part of the Magellanic Stream, its distance might be about 60 kpc. If there were no confining force except the self–gravity of the cloud, it would double its size in approximately 2×10^7 years.

Our high–resolution imaging of CHVC 120−20−443 provides some insights into the possible origin of this object. As noted in Sect. 4, the high–column–density cores in this source are concentrated in a semi–circular rim along the eastern periphery, in the direction of the M 31 disk. Furthermore, exceptionally broad linewidths, of 25 to 30 km s^{-1} *FWHM*, are seen in this rim feature, while enhanced linewidths, amounting to 15 to 20 km s^{-1}, are seen throughout the source. Of the thirteen CHVCs studied to date with arcmin resolution, only CHVC 110.6−07.0−466 has shown comparably broad linewidths in the CNM cores that are detected in interferometric data. Median linewidths in the CNM cores of CHVCs imaged by Wakker & Schwarz (1991), Braun & Burton (2000), and in this paper are only 6 km s^{-1}. As noted previously, it is not yet clear whether the broad linewidths are intrinsic, or due to a large-scale geometric effect. One possibility might be a large physical extent along the line–of–sight. Another curious circumstance is the large spatial offset of the brightest diffuse H I detected in the Green Bank 140–foot data toward the southeast of the CNM rim, as seen in Fig. 4. All of these observations suggest that CHVC 120−20−443 is in a different evolutionary state than the other CHVCs which have been studied. Wakker & Schwarz (1991) suggest a similarly different evolutionary state for CHVC 110.6−07.0−466. A distinct possibility seems to be a physical interaction of some type with M 31.

It is interesting to speculate how an observer in M 31 would see CHVC 120−20−443 if it were at the relative distance of 18 kpc. Given the properties of the cloud, the M 31 observer's perception of it could resemble the impression an earth-based observer has of the HVC Complexes A or C. For an observer located in the center of M 31, the cloud would extend over some 30° on the sky. Lower limits to the peak column densities that the observer would measure are determined by the ones measured in the WSRT observations, which have values of a few times 10^{19} cm^{-2}. The WSRT observations show a filamentary structure with several embedded higher–density clumps. The relative velocity of the object would be about 140 km s^{-1}, given the M 31 systemic velocity of −300 km s^{-1}. In order for this velocity to correspond to infall toward M 31 the object would have to be located beyond M 31, rather than between M 31 and the Galaxy. From our vantage point in the Galaxy, the HVC Complex A extends over about 30° on the sky, while Complex C extends over some 70°. Both have radial velocities of about −100 km s^{-1} in the Galactic Standard of Rest frame, and peak column densities of about 10^{19} cm^{-2} as measured in the Leiden/Dwingeloo survey. Concerning distances, we note that Complex A is well constrained to lie between 8 and 10 kpc (van Woerden et al. 1999; Wakker 2001), while only a few lower limits are available for Complex C. Although these clouds do not agree perfectly regarding their observable HI properties, they resemble each other sufficiently that it seems plausible to speculate about a similar physical origin.

Given the substantial projected distance of CHVC 120−20−443 from M 31, an origin in a galactic fountain within that galaxy seems unlikely. In a galactic fountain, gas which is heated and ionised by supernova explosions rises to higher z–height, either buoyantly or driven by subsequent supernovae, where it finally condenses and returns in free fall back toward the galactic disk (see Shapiro & Field 1976; Bregman 1980). Simulations carried out by de Avillez (2000) suggest that the height of this condensation process is at most several kpc above the stellar disk. CHVC 120−20−443 is located substantially further away from the stellar disk of M 31. Because the driving force of a galactic fountain is provided by supernova explosions, which are concentrated in OB–associations, it is remarkable that only one such cloud would be seen. The location of CHVC 120−20−443 is also not correlated with any region in M 31 of particularly active star formation (see Pellet et al. 1978), making this scenario appear unlikely.

A tidal origin for CHVC 120−20−443, related to either M 32 or NGC 205, is worth considering. Ibata et al. (2001) have discovered a tidal stream of metal–rich stars extending several degrees toward the south of M 31. They consider the dwarfs M 32 or NGC 205 as possibly responsible for the origin for the stream. The angular extent of the stellar stream toward the south is comparable to the separation of CHVC 120−20−443 from the center of M 31 toward the north. Together these systems might trace portions of the same orbital path. However, the measured radial velocity of the cloud is difficult to reconcile with those of the dwarfs. Both dwarfs have positive radial velocities with respect to M 31 (+155 km s^{-1} in the case of M 32 and +59 km s^{-1} in the case of NGC 205) whereas the high–velocity cloud has a negative relative velocity of −145 km s^{-1}. According to the distances listed in Mateo (1998), NGC 205 is located beyond M 31. Combined with its positive velocity with respect to M 31, it could be moving away from its peri–center passage. During closest approach, the gas could have been stripped, either by ram–pressure stripping or by tidal disruption. However, the deceleration of the gas by some 200 km s^{-1} would need to be accounted for. Realistic hydrodynamic simulations of such encounters might be illuminating.

Finally, the cloud could be part of a Local Group population of H I condensations within low–mass dark-matter halos, as described in the Local Group deployment model of CHVCs (Blitz et al. 1999; Braun & Burton 1999). Analysis of the all–sky population of CHVCs performed by de Heij et al. (2002b) has resulted in a self–consistent scenario whereby the observed CHVCs are part of a power–law distribution in baryonic mass (with slope −1.7) coupled to a steeper power–law (with slope −2) in dark mass. Only within the H I mass range of some $10^{5.5}$ to 10^7 $M_\odot$ are the objects stable against complete ionization by the intergalactic radiation field on the one hand (at low mass), and stable to internal star formation on the other (at high mass). The best–fitting simulated spatial distributions are centered on each of the Galaxy and M 31 with a spatial Gaussian dispersion of some 150 kpc. The majority of currently detected CHVCs belong to the relatively nearby swarm centered on the Galaxy. Only a small fraction of the M 31 sub–concentration of CHVCs is predicted to have been bright enough for detection in the current H I surveys. At the distance of M 31, CHVC 120−20−443 has an H I mass of about 10^7 $M_\odot$, putting it at the high–mass end of the distribution. If the projected separation with respect to M 31 is a measure for its real distance, then the cloud is sufficiently close to be strongly perturbed by the ram–pressure of its motion through a gaseous halo around M 31 (see de Heij et al. 2002b). The observed extreme CNM linewidths in this object, and the significant displacement of the diffuse gas in the direction of M 31 with respect to the core components, may both be evidence for such an ongoing perturbation.

Of all of the CHVCs extracted by de Heij et al. (2002a) from the LDS together with those found in the HIPASS material by Putman et al. (2002) and comprising an all–sky sample, only six have a velocity more extreme than $|V_{\rm LSR}| = 400$ km s^{-1}. All of these objects have negative velocities, and all lie at northern declinations; they constitute the population of clouds often called VHVCs. Arguments that this kinematic envelope is not an artifact of the observational parameters are given by de Heij et al. (2002b). (The most extreme positive–velocity CHVC is the HIPASS object CHVC 258.2−23.9+359; the most extreme negative–velocity CHVC at southern declinations is CHVC 125.1−66.4−353.) The most extreme–velocity CHVCs are the following, using the designation given by de Heij et al. and, in parenthesis, the entry numbers from the catalogs of Wakker & van Woerden (1991), Braun & Burton (1999), and de Heij et al. (2002a): CHVC 103.4−40.1−414 (WW#491, deH#57), CHVC 107.7−29.7−429 (WW#437, BB#22, deH#59), CHVC 108.3−21.2−402 (WW#389, BB#23, deH#60), CHVC 110.6−07.0−466 (WW#318, BB#24, deH#61), CHVC 113.7−10.6−441 (WW#330, BB#25, deH#62), and Davies' cloud CHVC 120.2−20.0−444 (deH#68). These CHVCs cluster near the direction of the barycenter of the Local Group, and are characteristically faint and small: they are likely to play an important role in the continuing discussion of the Local Group hypothesis.

The simulations of the Local Group hypothesis reported by de Heij et al. (2002b) support the prediction that a substantial number of additional CHVCs at extreme velocities will be found in the general direction of the Local Group barycenter, i.e. near M 31, when the sensitivity of the available H I survey data is improved. The unusual properties of Davies' cloud may be revealed by other objects. Two of the extreme–velocity objects (both discovered by Hulsbosch, 1978), namely CHVC 113.7−10.6−441 and CHVC 110.6−07.0−466, have been subject to synthesis imaging by Wakker & Schwarz (1991). It is interesting to note that Wakker & Schwarz state that the properties of these CHVCs differ considerably from the properties of the extended HVCs which they also partly imaged. CHVC 110.6−07.0−466 showed the same broad linewidth properties as we have found here for Davies' cloud. It is plausible that the two objects have undergone a similar evolutionary experience.

5.4. Summary and conclusions

We have imaged five CHVCs in H I with arcmin angular resolution and km s^{-1} spectral resolution using the Westerbork Synthesis Radio Telescope. These five images raise to 13 the number of CHVCs which have been subject to synthesis mapping, including the two compact objects studied by Wakker & Schwarz (1991) and the six studied by Braun & Burton (2000). These objects have a characteristic morphology, consisting of one or more quiescent, low–dispersion compact cores embedded in a diffuse warm halo. The compact cores can be unambiguously identified with the cool neutral medium of condensed atomic hydrogen, since their linewidths are significantly narrower than the thermal linewidth of the warm neutral medium. Because of the limited sensitivity to diffuse emission inherent to interferometric data, the warm medium is not directly detected in the synthesis observations discussed here. Supplementary total–power data, which is fully sensitive to both the cool and warm components of H I, is available for all sources for comparison, although with angular resolutions that vary from 3′ to 36′. The fractional H I flux in compact CNM components varies from 4% to 16% in our sample. All objects have at least one local peak in the CNM column density which exceeds about 10^{19} cm^{-2} when observed with arcmin resolution. The accompanying diffuse WNM halo reaches comparable peak column densities, of about 1–2 $\times$ 10^{19} cm^{-2}, external to these peaks (Burton et al. 2001). It is conceivable that a WNM halo column density of $1–2\times10^{19}$ cm^{-2} is a prerequisite for the long–term survival of these sources.

One object in our sample, CHVC 120−20−443 (Davies' cloud), lies in close projected proximity to the disk of M 31. This object is characterized by extremely broad linewidths in its CNM concentrations, which are 5 to 6 times broader than the median value found in the 13 objects studied to date at comparable resolutions. The CNM concentrations lie in an arc on the edge of the source facing the M 31 disk. The diffuse H I component of this source, seen in total–power data, has a large positional offset in the direction of the M 31 disk. All of these attributes suggest that CHVC 120−20−443 is in a very different evolutionary state than the other CHVCs which have been studied, with the possible exception of CHVC 110.6−07.0−466 (Hulsbosch's cloud), imaged by Wakker & Schwarz (1991) and

shown to also have broad linewidth CNM clumps. A distinct possibility seems to be a physical interaction of some type with M 31. The most likely form of this interaction might be ram–pressure or tidal–stripping of one of M 31's visible dwarf companions, M 32 or NGC 205, or of a dark companion with an associated H I condensation.

Acknowledgements. The Westerbork Synthesis Radio Telescope is operated by the Netherlands Foundation for Research in Astronomy under contract with the Netherlands Organization for Scientific Research. The National Radio Astronomy Observatory is operated by Associated Universities, Inc., under contract with the US National Science Foundation. The Arecibo Observatory is part of the National Astronomy and Ionosphere Center, which is operated by Cornell University under contract with the US National Science Foundation. The Parkes telescope is part of the Australia Telescope which is funded by the Commonwealth of Australia for operation as a National Facility managed by CSIRO.

References

Barnes, D. G., Staveley–Smith, L., de Blok, W. J. G., et al. 2001, MNRAS, 322, 486
Blitz, L., Spergel, D. N., Teuben, P. J., Hartmann, D., & Burton, W. B. 1999, ApJ, 514, 818
Burton, W. B., Braun, R., & Chengalur, J. N. 2001, A&A, 369, 616
Braun, R., & Walterbos, R. A. M. 1992, ApJ, 386, 120
Braun, R. 1995, A&AS, 114, 409
Braun, R. 1997, ApJ, 484, 637
Braun, R., & Burton, W. B. 1999, A&A, 341, 437
Braun, R., & Burton, W. B. 2000, A&A, 354, 853
Bregman, J. N. 1980, ApJ, 236, 577
Brüns, C., Kerp, J., & Pagels, A. 2001, A&A, 370, 26
Corbelli, E., & Salpeter, E. E. 1993, ApJ, 419, 104
Davies, R. D. 1975, MNRAS, 170, 45
de Avillez, M. A. 2000, Ap&SS, 272, 23
de Heij, V., Braun, R., & Burton, W. B. 2002a, A&A, in press [astro-ph/0201249]
de Heij, V., Braun, R., & Burton, W. B. 2002b, A&A, in press [astro-ph/0206306]
Draine, B. T. 1978, ApJS, 36, 595
Eichler, D. 1976, ApJ, 208, 694
Einasto, J., Haud, U., Jôeveer, M., & Kaasik, A. 1976, MNRAS, 177, 357
Field, G. B., Goldsmith, D. W., & Habing, H. J. 1969, ApJ, 155, L149
Giovanelli, R., Verschuur, G. L., & Cram, T. 1973, A&AS, 12, 209
Hartmann, D., & Burton, W. B. 1997, Atlas of Galactic Neutral Hydrogen (Cambridge University Press)
Hulsbosch, A. N. M. 1978, A&A, 66, L5
Ibata, R., Irwin, M., Lewis, G., Ferguson, A. M. N., & Tanvir, N. 2001, Nature, 412, 49
Klypin, A., Kravtsov, A. V., Valenzuela, O., & Prada, F. 1999, ApJ, 522, 82
Maloney, P. 1993, ApJ, 414, 41
Mateo, M. 1998, ARA&A, 36, 435
Moore, B., Ghigna, S., Governato, G., et al. 1999, ApJ, 524, L19
Muller, C. A., Oort, J. H., & Raimond, E. 1963, C. R. Acad. Sci. Paris, 257, 1661
Pellet, A., Astier, N., Viale, G., et al. 1978, A&AS, 31, 439
Putman, M. E., & Gibson, B. K. 1999, PASA, 16, 70
Putman, M. E., de Heij, V., Stavely–Smith, L., et al. 2002, AJ, 123, 873
Shapiro, P. R., & Field, G. B. 1976, ApJ, 205, 762
Verschuur, G. L. 1969, ApJ, 156, 771
Wakker, B. P. 2001, ApJS, 136, 537
Wakker, B. P., & Schwarz, U. 1991, A&A, 250, 484
Wakker, B. P., & van Woerden, H. 1991, A&A, 250, 509
Wakker, B. P., & van Woerden, H. 1997, ARA&A, 35, 217
Wakker, B. P., van Woerden, H., & Gibson, B. K. 1999, in Stromlo Workshop on High–Velocity Clouds, ed. B. K. Gibson, & M. E. Putman, ASP Conf. Ser., 166, 311
Wakker, B. P., Vijfschaft, B., & Schwarz, U. J. 1991, A&A, 249, 233
Williams, D. R. W. 1973, A&AS, 8, 505
van Woerden, H., Schwarz, U. J., Peletier, R. F., Wakker, B. P., & Kalberla, P. M. W. 1999, Nature, 400, 138
Wolfire, M. G., McKee, C. F., Hollenbach, D., & Tielens, A. G. G. M. 1995, ApJ, 453, 673